Scripta Materialia 139 (2017) xxx–xxx

Contents lists available at ScienceDirect

Scripta Materialia

journal homepage: www.elsevier.com/locate/scriptamat

Acoustic emissions associated with stress-induced twin boundary mobility in Fe_7Pd_3 ferromagnetic shape memory alloys

A.J. Bischoff[a,*], S.G. Mayr[a,b]

[a] Leibniz Institute of Surface Modification (IOM), Permoserstraße 15, Leipzig 04318, Germany
[b] Division of Surface Physics, University of Leipzig, Linnéstraße 5, Leipzig 04103, Germany

ARTICLE INFO

Article history:
Received 7 May 2017
Received in revised form 14 June 2017
Accepted 15 June 2017
Available online xxxx

Keywords:
Shape memory effect
Twinning dislocations
Acoustic emission
Nanoindentation

ABSTRACT

Twin boundary mobility is an essential prerequisite for the occurrence of magnetic field induced reversible strains in the ferromagnetic shape memory alloy Fe_7Pd_3. To study the behavior of twin boundaries, an abrupt movement of these structures is locally induced by nanoindentation while concomitant acoustic emissions are detected. In martensitic Fe_7Pd_3 bulk sample acoustic emissions can be correlated to pop-in events in the force-depth curves of the nanoindentation indicating twin boundary movement. In contrast, analogous experiments on freestanding Fe_7Pd_3 thin films indicate an insufficient hindering of twin boundary movements within the samples so that no abrupt dislocation displacement bursts take place.
© 2017 Acta Materialia Inc. Published by Elsevier Ltd. All rights reserved.

Ferromagnetic shape memory (FSM) alloys are captivating smart functional materials which feature reversible strains of several percent in an applied magnetic field. These macroscopic shape changes are induced by the reorientation of twin variants in the martensitic phase [1] and their magnitude depends essentially on twin boundary mobility, magnetic anisotropy and the axis-ratio of the crystal lattice [2,3]. In this context, the ferromagnetic shape memory alloy Fe_7Pd_3 is of particular interest because of its high ductility, low brittleness [4], and biocompatibility [5] enabling the use of this alloy in miniaturized actuation devices in micromedicine.

The occurrence and magnitude of the FSM effect in a material depend essentially on twin boundary mobility wherefore the behavior of these structures is of particular scientific interest. A possibility to experimentally activate the movement of twin boundaries within a sample is given by nanoindentation. With this technique, a load is applied locally inducing discrete and abrupt events, e.g., stress-induced martensitic transformations or deformation bursts due to reorientation of martensitic variants in shape memory materials as has been investigated for instance in NiTi [6–8] and CuAlBe [9–11]. These so called pop-in or pop-out events are associated with cascade-like shapes of the loading and unloading nanoindentation force-depth curves, respectively. The activated region is thereby spatially limited as shown by finite element modeling of martensitic transformations induced by nanoindentation in NiTi [8]. Here the transformed volume within a sample has a radius of about two times the contact radius of the nanoindenter tip if the indentation takes place in the elastic deformation regime.

In case of martensitic FSM samples, pop-in and pop-out events induced by nanoindentation are expected to originate from abrupt twin boundary movements due to the stress-induced reorientation of martensitic variants. However, cascade-like force-depth curves are also associated with other events such as crack formation, oxide film failure or dislocation nucleation. By additionally analyzing the acoustic emissions correlated with pop-in or pop-out events induced by nanoindentation, both magnitude and type of the triggering event can be identified [12].

In Fe_7Pd_3 thin films, pop-ins have already been observed during nanoindentation [13] but have not yet been studied in detail. In this work, we present nanoindentation experiments performed on Fe_7Pd_3 samples which were placed on a piezo electric acoustic emission sensor. These measurements were conducted to induce locally the movement of twin boundaries within the samples and to use, thus, both force-depth curves and acoustic emission signals to gain a better understanding of twin boundary mobility in FSM alloys. To avoid measurements of stress-induced martensitic transformations, experiments were performed on Fe_7Pd_3 samples in martensitic phase in fct structure. In this particular phase, Fe_7Pd_3 shows both a reversible thermally induced phase transformation to austenite [14]

* Corresponding author.
E-mail addresses: alina.bischoff@t-online.de (A. Bischoff), stefan.mayr@iom-leipzig.de (S. Mayr).

http://dx.doi.org/10.1016/j.scriptamat.2017.06.028
1359-6462/© 2017 Acta Materialia Inc. Published by Elsevier Ltd. All rights reserved.

ARTICLE IN PRESS

and a magnetic field induced reorientation of martensitic variants due to the FSM effect [15].

A martensitic Fe_7Pd_3 bulk sample with a composition of $Fe_{71}Pd_{29}$ and a thickness of about 60 μm was fabricated using a splat-quenching technique, as described previously [16]. Therefore, a Fe-Pd ingot with a corresponding composition was prepared by an arc melting procedure and after solidification divided into segments of about 180 mg each. These pieces were then remelted in the arc melter at 600 mbar and splatted between two Cu pistons to ensure rapid solidification. The splat sample exhibited homogeneous surfaces due to polishing with a strong columnar structure and visible surface twinning structures.

Single crystalline Fe_7Pd_3 thin films with a thickness of 500 nm were prepared with molecular beam epitaxy, as basically described previously [17]. The samples were grown from two independent rate-controlled electron beam evaporators with a total rate of 0.15 nm/s on MgO(100) substrates at substrate temperatures of $\approx$ 695 °C. The phase transformation temperature from austenite to martensite of the grown thin films is slightly above room temperature varying a few kelvins due to off-stoichiometry and stresses [18]. Subsequently, the MgO substrates were dissolved in a saturated sodium bicarbonate $NaHCO_3$ solution to obtain freestanding thin films [19]. The used specimens resided in fct-martensitic phase at room temperature as determined with X-ray diffraction (XRD) using a Seifert XRD 3003 PTS. Additionally, the phase of the samples was identified by the distinct degree of tetragonality given by the c/a-axis ratio which was determined with atomic force microscopy (AFM) measurements of the surface relief of the samples using a Veeco Icon Dimension. The thin film specimens showed c/a-ratios of 0.94–0.96, confirming fct-martensitic phase.

Nanoindentation measurements were performed with an ASMEC Universal Nanomechanical Tester device (UNAT) in a classical fast hardness mode according to IOS 14577 using a Berkovich tip of $\approx$ 0.2 μm tip radius. Additionally, measurements on some thin film samples were performed with a dynamical "quasi-continuous-stiffness-measurement" (QCSM) mode [20]. During the loading segment of this mode, a sinusoidal oscillation with a frequency of about 5 Hz is switched on for in total 48 short dwell times of 3 s duration each while the normal force is kept constant. The QCSM mode allows to determine the elastic modulus of the sample depth dependently which is particularly interesting for thin film samples as indenter tip and substrate effects influence the measurement results at small and bigger depths, respectively. Relatively unaffected Young's moduli are, hence, only obtained in $\approx$ 40–50 nm depth in the case of 500 nm thin films.

For all measurements, samples were placed on top of a Vallen Systeme VS150-M passive piezo electric acoustic emission sensor with a frequency range of 100–450 kHz and a resonance frequency of 150 kHz. The combined measurement set-up is sketched in Fig. 1 and consisted of the acoustic emission sensor, the nanoindenter, a Vallen Systeme AEP3N preamplifier (49 dB gain), a Vallen Systeme DCPL2 signal decoupling box, a National Instruments NI USB 6361 DAQ data acquisition box, a 28 V_{DC} power supply and two computers. Data acquisition of the acoustic emission sensor is controlled with a LabView program and set to an acquisition rate of 150,000 data points/s. Background noise of the sensor amounts to about $\pm$ 15 mV. For sample attachment on the sensor the Electron Microscopy Sciences wash-away adhesive Crystalbond 555 was used with a flow point of 54 °C. For a part of the measurements on freestanding thin film samples, moistened films were mounted on the sensor with slight surface drying without using an adhesive. This sample attachment method was mainly used for nanoindentation measurements with the QCSM mode in order to exclude influences of the relatively soft adhesive on the depth dependent Young's moduli of freestanding Fe_7Pd_3 thin films.

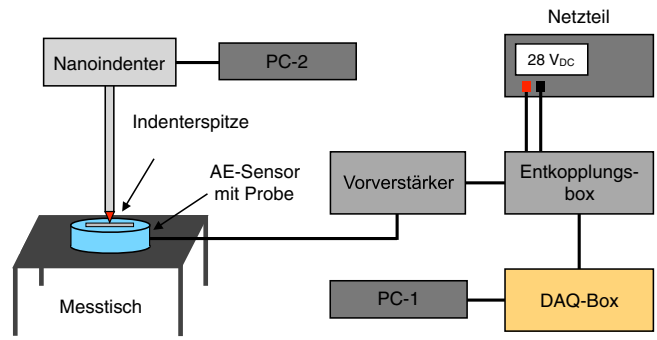

Fig. 1. Sketch of the set-up for the combined nanoindentation and acoustic emission measurements.

Acoustic emission signals were detected during nanoindentation measurements on the martensitic Fe_7Pd_3 splat at chosen maximal indentation forces of 10–100 mN. The loading part of each indentation lasted for 10 s, followed by 1 s creep time and a 4 s unloading segment. At higher maximal indentation forces, stronger acoustic signals were measured as shown in Fig. 2. The individual acoustic signals were associated with weakly defined pop-in events in the corresponding force-depth curves of the nanoindentation measurements.

The relatively low signal levels of both the acoustic and the nanoindentation measurements are caused by the polycrystalline character of the splat. Due to grain boundaries within the sample, more nucleation sources for twinning dislocations are present, however, these boundaries also hinder twin boundary mobility. In the twinned, fct-martensitic splat sample, twin boundary movement is, hence, attenuated resulting in relatively weak measurement signals.

Nanoindentation measurements on freestanding Fe_7Pd_3 thin films were performed at chosen maximal indentation forces of 0.5–5 mN with loading times of 1–10 s. During these measurements no acoustic signals were detected above or below the background noise of the acoustic emission sensor. Moreover, the force-depth curves of the nanoindentation measurements featured hardly ever cascade-like shapes in reasonable indentation depths. Apparently at the investigated force and time scales, twin boundary movement is either not strongly enough hindered within the material to occur in

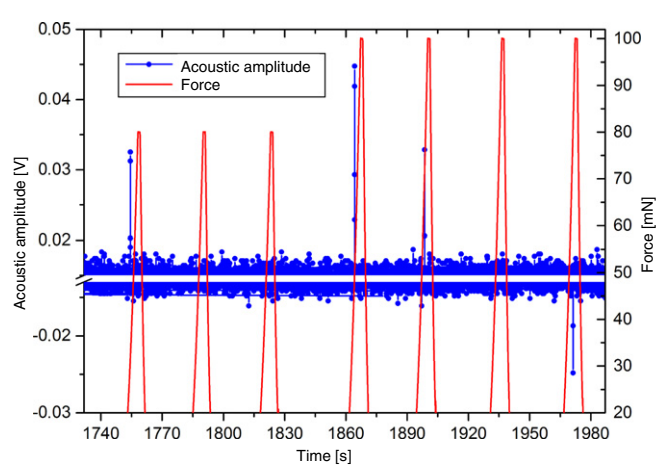

Fig. 2. Acoustic emission signals and force values of the nanoindentation measurement performed on a martensitic Fe_7Pd_3 splat.

Please cite this article as: A. Bischoff, S. Mayr, Acoustic emissions associated with stress-induced twin boundary mobility in Fe_7Pd_3 ferromagnetic shape memory alloys, Scripta Materialia (2017), http://dx.doi.org/10.1016/j.scriptamat.2017.06.028

ARTICLE IN PRESS

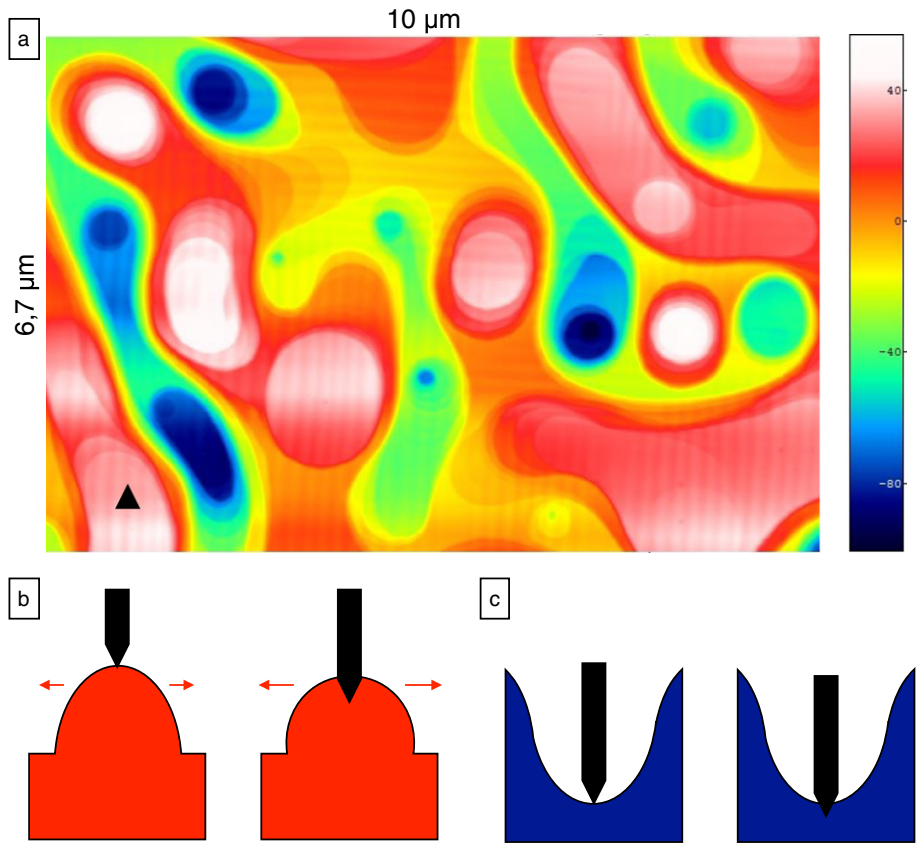

Fig. 3. AFM measurement of a freestanding martensitic Fe_7Pd_3 thin film with drawn in scaled indenter tip shape (a). Sketches of the behavior of material pile-ups (b) and vales (c) due to the indentation of the tip.

abrupt movement bursts (I) or is not taking place (II) or cannot be detected with the set-up due to its sensitivity (III).

(I): The first argument is supported by AFM measurements of the thin film topography as shown in Fig. 3a. The sample surfaces are characterized by material pile-ups and vales those areas are typically in the size range of the indenter tip (sketched in the figure as a black triangle). During the penetration process of the tip, scenarios as sketched in Fig. 3b and c, i.e., penetration in material pile-ups or vales can occur or even a scraping of the tip along the slope of a pile-up. In the relatively soft thin film, which features a Young's modulus of 5–16 GPa [13,21], stresses due to nanoindentation are compensated by spatial material deformation in the case of penetration in and scraping along material pile-ups. As a result no sufficiently high internal stresses are built up to induce abrupt reorientation of martensitic variants and twin boundary movement. However during nanoindentation at surface vales, one would expect the thin film samples to be stiffer and probably cascade-like force-depth dependencies as observed for the investigated bulk sample. But even indentation procedures indicating locally higher elastic moduli were not unambiguously correlated with pop-in events.

(II): In general, twin boundary mobility can take place in Fe_7Pd_3 thin film samples as observed during tensile experiments [21]. So far, evidence for induced twin boundary mobility due to nanoindentation with correlated acoustic emission has only been observed in bulk samples but there is no apparent reason why twin boundaries movement should not be induced by nanoindentation in thin film samples as well.

(III): To estimate the expected signal strength of the acoustic emission caused by the movement of twinning dislocations within Fe_7Pd_3 thin films, we evaluated the corresponding radiated energy per cycle and length of dislocation according to Ref. [22]. For this calculation, one assumes that a dislocation is oscillating because of an inciting elastic wave of velocity u_0 and that this dislocation movement results in energy scattering. The amount of this scattered energy is expected to correspond roughly to the amount of energy emitted due to an abrupt movement of a dislocation within a solid. For the Fe_7Pd_3 splat with a Young's modulus of 54 GPa, as determined with nanoindentation, this energy amounts to $2.1 \cdot 10^{10} \cdot u_0 \cdot$ N/m^2 (calculation based on a radial frequency of $2\pi \cdot 150$ kHz, a Poisson ratio of 0.33, a density of 8.91 g/cm^3 [23] and a lattice distance of the longer axis of the tetragonal unit cell of 382 pm). For a freestanding Fe_7Pd_3 thin film with a Young's modulus of 5–16 GPa [13,21], this estimation yields a radiated energy of $1.6 - 4.6 \cdot 10^9 \cdot u_0 \cdot$ N/m^2. Compared to the value determined for the splat, this result indicates that the acoustic emission caused by dislocation movement is about an order of magnitude smaller in a thin film sample. Hence, acoustic signals are most likely more difficult to detect in Fe_7Pd_3 thin films. Nonetheless, the estimated value is comparable to the radiated energy expected in indium samples which amounts to $3.1 \cdot 10^9 \cdot u_0 \cdot$ N/m^2 (calculation based on a radial frequency of $2\pi \cdot 150$ kHz, a Young's modulus of 11 GPa, a Poisson ratio of 0.45, a density of 7.31 g/cm^3 and a lattice distance of the

Please cite this article as: A. Bischoff, S. Mayr, Acoustic emissions associated with stress-induced twin boundary mobility in Fe_7Pd_3 ferromagnetic shape memory alloys, Scripta Materialia (2017), http://dx.doi.org/10.1016/j.scriptamat.2017.06.028

longer axis of the tetragonal unit cell of 495 pm [24]). In indium, stress-induced nucleation of twinning dislocations has been observed and corresponding acoustic signals have been detected [25]. With our set-up, relatively strong acoustic signals were detected during nanoindentation measurements with maximal forces of 800 mN on a indium bulk sample of (5×3 x 1) mm^3. We, thus, expect the sensitivity of our set-up to be sufficiently high to detect acoustic emission signals due to abrupt twin boundary movement in Fe_7Pd_3 thin films.

Nanoindentation measurements performed on freestanding Fe_7Pd_3 thin films showed strongly variating results regarding the reached maximal penetration depths and the calculated elastic moduli. The latter becomes particularly apparent during measurements with the QCSM mode at maximal forces of 0.5–2 mN which provided depth dependent Young's moduli data. In the depth range of interest of 40–50 nm, elastic moduli varied between about 2 GPa and up to 40 GPa with the average values at different maximal forces residing at 3.8–10.2 GPa.

These strong variations in Young's moduli can again be explained by the samples' topography, i.e., by material pile-ups and vales as shown exemplarily in Fig. 3a. The resulting influence on the penetration process of the tip was outlined above and is sketched in Fig. 3b and c. The small elastic moduli results can be ascribed to nanoindentations in and scraping of the tip along material pile-ups while the occasionally detected high moduli point to nanoindentations at surface vales.

The maximal penetration depths ranged between ≈ 200 nm up to several μm, due to sample topography and its influence on local elastic film properties. In the case of penetration depths exceeding the film thickness of 500 nm, displacement of trapped air took place causing these high depth values as no adhesive was used for sample mounting for these measurements.

Cascade-like force-depth curves as shown in Fig. 4 were only observed very infrequently. Here, the most unambiguous example for such a curve shape is shown. Out of about 1000 fast hardness and about 400 QCSM mode measurements performed on 4 different martensitic Fe_7Pd_3 thin film samples, this was the only distinct cascade-like curve detected while less than 10 other curves exhibited very weakly pronounced but possibly cascade-like shapes. This observation supports argument (I) outlined in the section above,

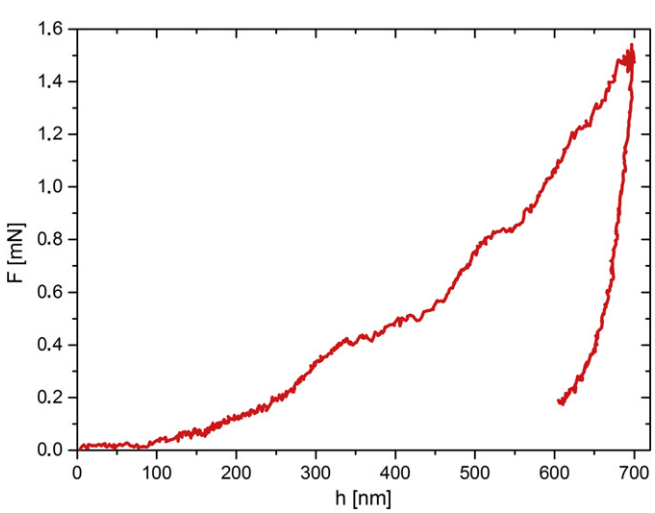

Fig. 4. Force-depth curve of a nanoindentation measurement on a freestanding martensitic Fe_7Pd_3 thin film indicating pop-in events. The measurement was performed with a loading segment of 10 s duration, a maximal force of 1.5 mN and with no use of an adhesive. Surface finding problems at the first 100–200 nm of the loading segment caused overestimated penetration depths.

suggesting that twin boundary movement is not strongly enough hindered within Fe_7Pd_3 thin films to occur in abrupt movement bursts.

In summary, we achieved to measure acoustic signals caused by abrupt movement of twin boundaries within a martensitic Fe_7Pd_3 bulk sample induced by nanoindentation with a combined measurement set-up. In freestanding Fe_7Pd_3 thin film samples, respective measurements did not result in the detection of both acoustic emissions and pop-in events in the force-depth curves of the nanoindentation measurements. We expect the reason for this behavior to be an insufficient hindering of twin boundary movements within the thin films so that no abrupt dislocation displacement bursts take place. This interpretation is supported by the rare occurrence of cascade-like force-depth curves observed during nanoindentation measurements.

This project was performed within the Leipzig Graduate School for Natural Sciences BuildMoNa, established within the German Excellence Initiative by the German Science Foundation (DFG). Financial support by the DFG-Project "MSMPUMP" was gratefully acknowledged. Thin film sample preparation was performed within the Research Internships in Science and Engineering (RISE) project of the German Academic Exchange Service (DAAD) by K. Hua. We further thank I. Kock for the preparation and characterization of the Fe_7Pd_3 bulk sample.

References

[1] K. Ullakko, J.K. Huang, C. Kantner, R.C. O'Handley, Appl. Phys. Lett. 69 (1996) 1966–1968.
[2] A.A. Likhachev, K. Ullakko, Phys. Lett. A 275 (2000) 142–151.
[3] A.A. Likhachev, A. Sozinov, K. Ullakko, Mater. Sci. Eng. A 378 (1-2) (2004) 513–518.
[4] J. Cui, T.W. Shield, R.D. James, Acta Mater. 52 (2004) 35–47.
[5] Y. Ma, M. Zink, S.G. Mayr, Appl. Phys. Lett. 96 (2010) 213703.
[6] A.J. Muir Wood, T.W. Clyne, Acta Mater. 54 (2006) 5607–5615.
[7] M. Arciniegas, Y. Gaillard, J. Peña, J.M. Manero, F.J. Gil, Intermetallics 17 (2009) 784–791.
[8] Y. Zhang, Y.-T. Cheng, D.S. Grummon, J. Appl. Phys. 101 (2007) 053507.
[9] C. Caër, E. Patoor, S. Berbenni, J.-S. Lecomte, Mater. Sci. Eng. A 587 (2013) 304–312.
[10] W.C. Crone, H. Brock, A. Creuziger, Exp. Mech. 47 (2007) 133–142.
[11] H.-S. Zhang, K. Komvopoulos, J. Mater. Sci. 41 (2006) 5021–5024.
[12] D.F. Bahra, W.W. Gerberich, J. Mater. Res. 13 (1997) 1065–1074.
[13] Y. Ma, S.G. Mayr, Acta Mater. 61 (2013) 6756–6764.
[14] M. Matsui, H. Yamada, K. Adachi, J. Phys. Soc. Jpn. 48 (1980) 2161–2162.
[15] R.D. James, M. Wuttig, Philos. Mag. A 77 (1998) 1273–1299.
[16] I. Kock, S. Hamann, H. Brunken, T. Edler, S.G. Mayr, A. Ludwig, Intermetallics 18 (2010) 877–882.
[17] L. Kühnemund, T. Edler, I. Kock, M. Seibt, S.G. Mayr, New J. Phys. 11 (2009) 113054.
[18] T. Edler, S. Hamann, A. Ludwig, S.G. Mayr, Scr. Mater. 64 (2011) 89–92.
[19] T. Edler, S. Mayr, Adv. Mater. 22 (2010) 4969–4972.
[20] Application note: Quasi continuous stiffness module QCSM, ASMEC GmbH, Radeberg, Germany.
[21] A.J. Bischoff, A. Landgraf, S.G. Mayr, Scr. Mater. 111 (2016) 76–80.
[22] J. Kiusalaas, T. Mura, Philos. Mag. 9 (1963) 1–7.
[23] H. Kato, Y. Liang, M. Taya, Scr. Mater. 46 (2002) 471–475.
[24] F. Cardarelli, Materials Handbook - A Concise Desktop Reference, Springer, London, 2008.
[25] S.L. Van Doren, R.B. Pond Sr, R.E. Green Jr, J. Appl. Phys. 47 (1976) 4242–4348.